Electron glass phase with resilient Zhang–Rice singlets in $LiCu_3O_3$

A. Consiglio,[1] G. Gatti,[2] E. Martino,[2] L. Moreschini,[3] J. C. Johannsen,[2] K. Prša,[2,4] P. G. Freeman,[2,5] D. Sheptyakov,[4] H. M. Rønnow,[2] R. Scopelliti,[6] A. Magrez,[2] L. Forró,[2,7] C. Schmitt,[8] V. Jovic,[3,9] C. Jozwiak,[3] A. Bostwick,[3] E. Rotenberg,[3] T. Hofmann,[1] R. Thomale,[1] G. Sangiovanni,[1] D. Di Sante,[10] M. Greiter,[1] M. Grioni,[2] and S. Moser[2,3,8,*]

[1]*Institut für Theoretische Physik und Astrophysik and Würzburg-Dresden Cluster of Excellence ct.qmat, Universität Würzburg, 97074 Würzburg, Germany*
[2]*Institute of Physics, Ecole Polytechnique Fédérale de Lausanne (EPFL), CH-1015 Lausanne, Switzerland*
[3]*Advanced Light Source (ALS), Berkeley, California 94720, USA*
[4]*Laboratory for Neutron Scattering and Imaging, Paul Scherrer Institut, 5232 Villigen PSI, Switzerland*
[5]*Jeremiah Horrocks Institute for Mathematics, Physics and Astronomy, University of Central Lancashire, Preston, PR1 2HE United Kingdom*
[6]*Institute of Chemical Sciences and Engineering, Ecole Polytechnique Fédérale de Lausanne (EPFL), CH-1015 Lausanne, Switzerland*
[7]*Stavropoulos Center for Complex Quantum Matter, Department of Physics & Astronomy, University of Notre Dame, Notre Dame, IN 46556 USA*
[8]*Physikalisches Institut and Würzburg-Dresden Cluster of Excellence ct.qmat, Universität Würzburg, Würzburg 97074, Germany*
[9]*Earth Resources and Materials, Institute of Geological and Nuclear Science, Lower Hutt 5010, New Zealand; MacDiarmid Institute for Advanced Materials and Nanotechnology, Wellington 6012, New Zealand*
[10]*Department of Physics and Astronomy, University of Bologna, Bologna, Italy*

(Dated: September 20, 2023)

$LiCu_3O_3$ is an antiferromagnetic mixed valence cuprate where trilayers of edge-sharing Cu(II)O ($3d^9$) are sandwiched in between planes of Cu(I) ($3d^{10}$) ions, with Li stochastically substituting Cu(II). Angle-resolved photoemission spectroscopy (ARPES) and density functional theory (DFT) reveal two insulating electronic subsystems that are segregated in spite of sharing common oxygen atoms: a Cu d_{z^2}/O p_z derived valence band (VB) dispersing on the Cu(I) plane, and a Cu $3d_{x^2-y^2}$/O $2p_{x,y}$ derived Zhang-Rice singlet (ZRS) band dispersing on the Cu(II)O planes. First-principle analysis shows the Li substitution to stabilize the insulating ground state, but only if antiferromagnetic correlations are present. Li further induces substitutional disorder and a paradigmatic 2D electron glass behavior in charge transport, reflected in a large 530 meV Coulomb gap and a linear suppression of VB spectral weight at E_F that is observed by ARPES. Surprisingly, the disorder leaves the Cu(II)-derived ZRS largely unaffected. This indicates a local segregation of Li and Cu atoms onto the two separate corner-sharing $Cu(II)O_2$ sub-lattices of the edge-sharing Cu(II)O planes, and highlights the ubiquitous resilience of the entangled two hole ZRS entity against impurity scattering.

The two principal oxides of copper, cuprous oxide Cu_2O and cupric oxide CuO, widely differ in their physical and spectroscopic properties [1]. Cu_2O contains monovalent Cu(I) ions with a completely filled Cu $3d$ shell and is a non-magnetic band insulator. CuO, however, contains divalent Cu(II) ions with an open Cu $3d^9$ shell, and is an antiferromagnetic (AFM) charge-transfer insulator [2]. Its lowest energy hole excitations have mixed $3d^9\underline{L}$ and $3d^8$ character, where $\underline{L}$ stands for ligand oxygen hole [3, 4], and are a matter of longstanding scientific debate [5].

In the low dimensional cuprates, the Cu(II) ions are typically coordinated by four oxygen atoms, forming rectangular CuO plaquettes (Fig. 1 c). These constitute building blocks of one (1D) or two dimensional (2D) networks, with adjacent plaquettes sharing either one- (corner-sharing) or two oxygen atoms (edge-sharing). In the corner-sharing configuration, the angle of the Cu-O-Cu bond is typically close to 180°, giving rise to super-exchange interaction and AFM [6]. Doping a low-energy hole into the O $2p$ sub-lattice, its spin entangles with the Cu $3d_{x^2-y^2}$ hole, forming a local singlet of ${}^1A_1$ symmetry and mainly $d^9\underline{L}$ character, with each hole in b_{1g} symmetric one-particle wave-functions (one in the $d_{x^2-y^2}$ orbital of Cu(II), the other one in an appropriate linear combination of the adjacent oxygen $p_{x,y}$ orbitals) [3]. This entangled two hole composite quasi-particle (QP), commonly dubbed Zhang-Rice singlet (ZRS), effectively disperses on the 2D Cu(II) sub-lattice assuming a bandwidth that is proportional to the super-exchange energy $J \sim 4t^2/U \sim 130$ meV, and is described by effective one band Hubbard or t-J Hamiltonians [3, 4, 7]. While this establishes the spectral equivalence of the ZRS and a one-electron excitation, their eigenstate profiles still differ substantially. As a consequence, phenomena that involve the explicit spatial distribution of the ZRS QP, such as impurity scattering, are expected to be subject to significant corrections. In the edge sharing configuration, the Cu-O-Cu bond angle is close to 90° and the super-exchange interaction is suppressed to values $J \sim 10$ meV [6, 8–10]. In this configuration, the ZRS wave-functions of adjacent plaquettes are orthogonal, and a ZRS dispersion cannot stabilize [11, 12].

Coupling a Cu(II)-oxide to Cu(I) adds additional complexity and can lead to novel electronic phenomena. This was recently exemplified by angle-resolved photoemission spectroscopy (ARPES) experiments on $LiCu_2O_2$, a mixed-valence compound where 1D edge-sharing chains of $Cu(II)O_4$ are coupled to 2D square lattices of Cu(I) ions through hybridization with common oxygens [13]. While the Cu(I) and Cu(II)

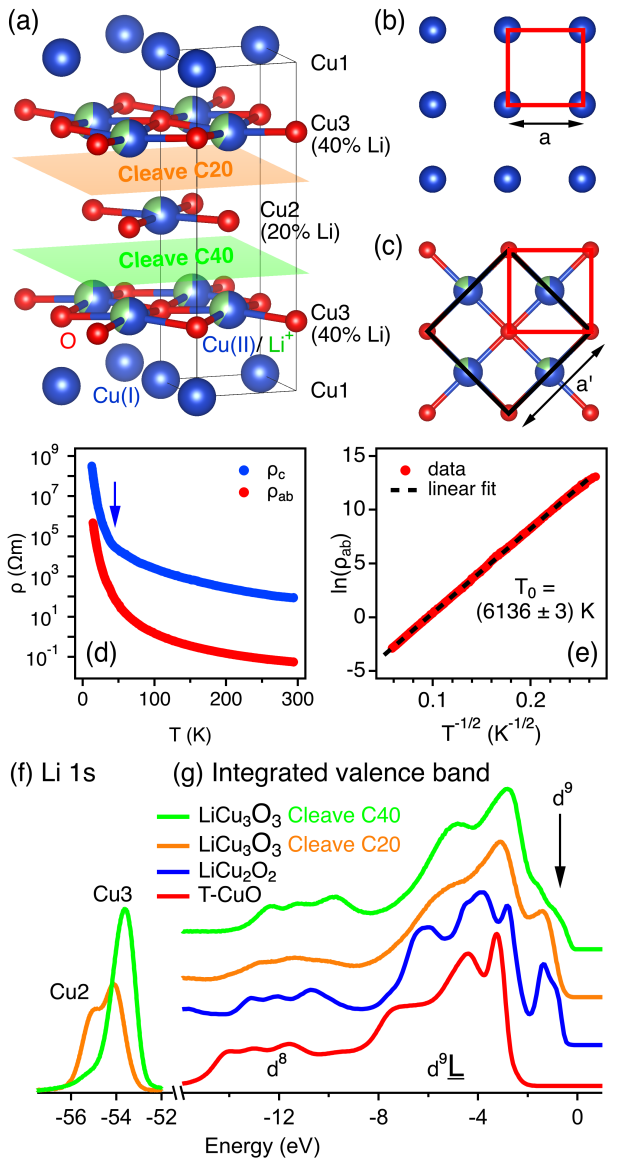

FIG. 1. (a) $LiCu_3O_3$ crystal structure, UC and natural cleavage planes. (b) Cu(I) form a square lattice with periodicity a (red square). (c) In a Cu(II) plane, edge-sharing CuO_4 plaquettes form a 2D square lattice with the same periodicity. The black square is the non-primitive $c(2 \times 2)$ UC. Li stochastically substitutes Cu(II) according to the stoichiometric ratios in (a). (d) In-plane (red) and out-of-plane (blue) DC resistivity of $LiCu_3O_3$. (e) The natural logarithm of the in plane resistivity scales as $T^{-1/2}$ with slope $\sqrt{T_0}$. (f) Li $1s$ spectra of both $LiCu_3O_3$ cleaves ($h\nu = 100$ eV). (g) Integrated VB spectra of both $LiCu_3O_3$ cleaves, compared to results from $LiCu_2O_2$ (blue [13]) and T-CuO (red [11]).

based structural sub-units retain their individual electronic character, the electronic structure was still found to be non-trivial, with an experimental bandwidth broadening of the Cu(I)-derived valence band (VB) of 250% with respect to predictions of DFT. The purely edge-sharing Cu(II)O_2 chains in $LiCu_2O_2$, however, do not support the formation of ZRSs. We thus anticipate intriguing electronic effects in materials combining corner-sharing 2D networks of Cu(II)O with Cu(I).

Such a system is embodied in the mixed-valence cuprate $LiCu_3O_3$, the least studied member within the lithium copper oxide family. Its tetragonal crystal structure (P4/mmm, $a = 2.81$ Å, $c = 8.89$ Å) is shown in Fig. 1 (a) [15–18]. Ignoring the lithium, the 3D unit cell (UC, black) consists of trilayers of Cu(II)O (Fig. 1 c) sandwiched between square lattice planes of Cu(I) (Fig. 1 b). The trilayers are structurally similar to tetragonal copper oxide (T-CuO), an epitaxial stack of Cu(II)O planes with both edge- and corner-sharing properties [11], yet with smaller out-of-plane to in-plane Cu(II)-O bond-length ratio of 1.22 vs. 1.37 in T-CuO. Due to the staggering along the crystal c-axis (Fig. 1 a), the Cu(II) species of the Cu2 and the Cu(I) of the Cu1 share common oxygen ligands within the two equivalent Cu3 planes. As we show here, $LiCu_3O_3$ is thus a hybrid containing a re-normalized Cu(I)-derived VB similar to $LiCu_2O_2$ [13] that is electronically separated from a Cu(II)O-derived ZRS as found in T-CuO [11].

The Li^+ ions stochastically substitute the Cu(II) species and add additional complexity, with $\sim 20\%$ Li per Cu site in the Cu2 plane, and $\sim 40\%$ Li per Cu site in the Cu3 plane [15, 16, 18]. As seen in Figs. 1 (d) and (e), this dis-order – along with long range Coulomb interactions – gov-erns the temperature dependence of direct electrical current (DC). In particular, the in-plane resistivity ρ_{ab} scales according to an Efros-Shklovskii variable range hopping law $\rho \propto \exp(\sqrt{T_0/T})$ [19–21] with characteristic temperature $T_0 = (6136 \pm 3)$ K, demonstrating the presence of a large Coulomb gap of $k_B T_0 \sim 530$ meV from 15 K to at least 300 K. T_0 also provides an upper bound of the charge carriers' localization length $\xi \leq 1.7$ nm $\sim 6a$ [18, 22, 23], which indicates strong charge localization and in-plane conduction to be dominated by slow hopping rather than fast diffusion processes [18]. Out-of-plane resistivity ρ_c and with it the aver-age out-of-plane bond resistance exceeds ρ_{ab} by about three orders of magnitude and at ~ 45 K (blue arrow) transitions from an Efros-Shklovskii to a Mott variable range hopping regime [18, 24, 25]. $LiCu_3O_3$ is thus a paradigmatic 2D elec-tron glass, i.e., an Anderson insulator subject to strong disor-der and Coulomb interactions [22, 23, 26, 27].

Despite the impact of substitutional disorder on resistivity, neutron scattering and SQUID magnetization measurements show Cu(II) derived long range AFM order below $T_N \sim 124$ K [18]. ARPES reveals both the Cu(I) VB and the Cu(II)O ZRS bands to remain surprisingly intact – a phenomenon that exact diagonalization (ED) and DFT calculations ascribe to a kinetic energy driven segregation of Li and Cu(II) species onto separate corner-sharing CuO_2 sub-lattices. The VB, however, exhibits a soft, linear Coulomb gap when tuned to the Fermi energy (E_F), an independent surface spectroscopic hallmark of the electron glass behavior that we discussed within the scope of transport right above [28, 29].

Let us first focus on the Li $1s$ angle integrated photoemission spectra of $LiCu_3O_3$ single crystals cleaved in ultra high vacuum (UHV) (Fig. 1 f). We distinguish two natural

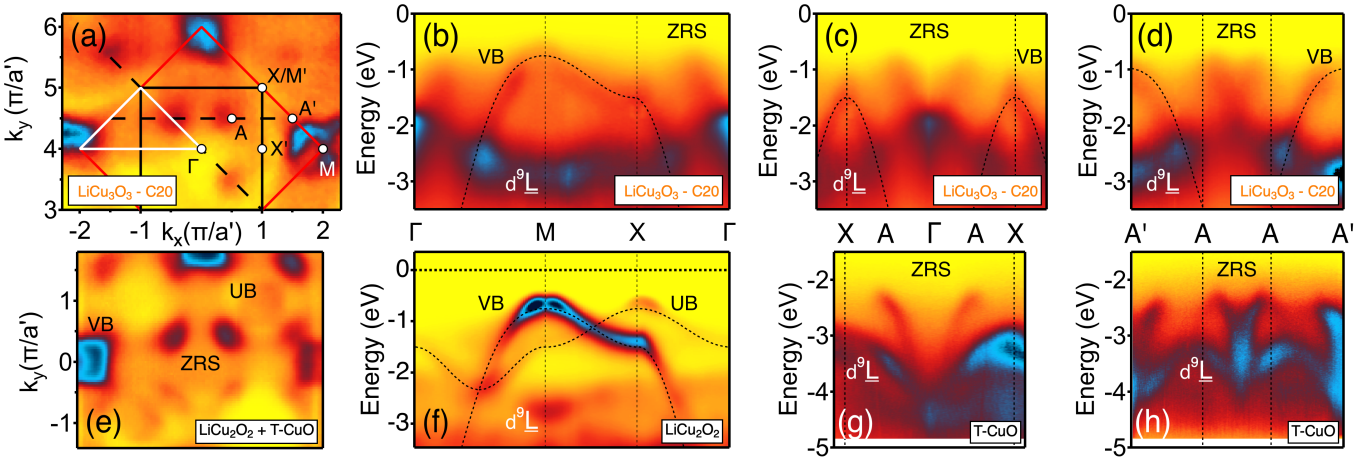

FIG. 2. (a) ARPES CE map of $LiCu_3O_3$ - C20 ($h\nu = 150$ eV, $T = 150$ K) at $E = -0.7$ eV. Red and black squares are BZs corresponding to the UCs defined in Fig. 1 (c). As at normal photo-electron emission, the ZRS is suppressed [11, 14], we show data centered around $(k_x, k_y) = (0, 4\pi/a')$. (b) ARPES dispersion along the white triangular path in (a), compared to results from $LiCu_2O_2$ in (f). The latter also exhibits an *Umklapp* band (UB) not present in $LiCu_3O_3$ [13]. (c) and (d) show dispersions along the black dashed lines in (a), and compare directly to the ZRS of T-CuO in (g) and (h) [11]. (e) Artificial sum of ARPES CE cuts of $LiCu_2O_2$ [13] and T-CuO [11].

cleavage planes that terminate the compound with planes Cu2 (cleave C20) and Cu3 (cleave C40), respectively (Fig. 1 a). While C20 reveals two peaks related to Li species in both the Cu2 (-55.08 eV) and the underlying Cu3 planes (-54.05 eV), C40 exhibits the single Li peak of the Cu3 plane (-53.60 eV), shifted by ~ 0.4 eV to lower binding energy w.r.t. C20 due to surface band bending [31]. VB spectra of both terminations in Fig. 1 (g) compare well to results obtained on T-CuO [11] and $LiCu_2O_2$ [13], exhibiting the characteristic of a correlated charge transfer insulator: a manifold of Cu-derived d^8 states at ~ -12 eV and an O-derived $d^9\underline{L}$ band around ~ -4 eV. Consistent with the Li $1s$ core level, the VB features of C40 are shifted upwards with respect to C20, with finite spectral weight at E_F leading to charge screening that produces the asymmetric line shape in the Li $1s$ peak [30]. Distinct from T-CuO, both $LiCu_2O_2$ and $LiCu_3O_3$ exhibit additional features within the charge-transfer gap (arrow).

We examine these features in the ARPES constant energy (CE) map of Fig. 2 (a), taken from C20 at $E = -0.7$ eV. In addition to the primitive Brillouin zone (BZ, red square) and high symmetry points of $LiCu_3O_3$, and consistent with our notation for T-CuO in Ref. 11, we define the mid-point X' between Γ and M (the X point of the reduced BZ of a corner-sharing CuO_2 sub-lattice, black), and pairs of points A, A' that are symmetric with respect to the XX'X line. We observe two sets of spectral features: First, intense spectral contours centered at the M points of the primitive BZ reflect the periodicity of the crystallographic surface UC (red in Fig. 1 b,c). Second, weaker spectral lobes are observed at the A-points, i.e., at $(\pm\pi/2a', \pm\pi/2a')$ with respect to the reduced BZ, corresponding to a $\sqrt{2}$ times larger and 45° rotated real space UC with lattice constant $a' = a\sqrt{2}$ (black in Fig. 1 c). The band dispersion along the high-symmetry contour ΓMXΓ (white triangle in Fig. 2 a) in Fig. 2 (b) shows two sets of bands [18]: First, a VB of bandwidth ~ 3.4 eV and maximum at ~ -0.7 eV that forms the contours at M in panel (a). By analogy with $LiCu_2O_2$ in Fig. 2 (f) [13] and confirmed by DFT [18], this band is of mostly Cu(I) d_{z^2} and adjacent O p_z character, and emerges from a broad and relatively flat $d^9\underline{L}$ manifold at around -2.3 eV [4]. Second, faint lobes at A and A' in panel (a) mark the onset of the ZRS at ~ -0.7 eV in (b) [2]. As seen in the E vs. $k_{\|}$ cuts of panels (c,d), it is similar to the ZRS in T-CuO shown in (g,h), where the Cu(II) atoms also form mixed edge and corner-sharing CuO planes. Both VB and ZRS exhibit negligible k_z dispersion in photon energy dependent ARPES and are thus clearly 2D [18].

Based on these experimental observations, we conjecture the low-energy electronic structure of $LiCu_3O_3$ to host two segregated electronic subsystems: (i) a ZRS band primarily associated to Cu(II) $d_{x^2-y^2}$ and O $p_{x,y}$ orbitals that propagates on the Cu(II)O planes and shows a similar dispersion as in T-CuO; and (ii) a VB of Cu(I) d_{z^2} and O p_z orbital character that propagates on the Cu(I) lattice and displays a similar bandwidth and dispersion as in $LiCu_2O_2$. Indeed, the remarkable resemblance of Fig. 2 (a) with an artificial sum of $LiCu_2O_2$ [13] and T-CuO [11] data in Fig. 2 (e) illustrates the composite nature of the $LiCu_3O_3$ electronic structure [32].

Surprises come at a close inspection of ARPES measured on C40. A CE map in Fig. 3 (a), this time collected at -0.4 eV, is similar to the CE map of C20 at -0.7 eV in Fig. 2 (a), showing both the onset of the Cu d_{z^2}/O p_z de-rived VB and of the Cu $3d_{x^2-y^2}$ /O $2p_{x,y}$ derived ZRS. In contrast to C20, however, upwards surface band bending – as commonly present in transition metal insulators [31] – renders the VB slightly p-doped, producing the remnant Fermi surface shown in panel (b). An ARPES cut along the dashed line in (b) shows spectral weight to not quite reach, and in fact, even repel from E_F, resulting in a *squashed* VB maximum in panel

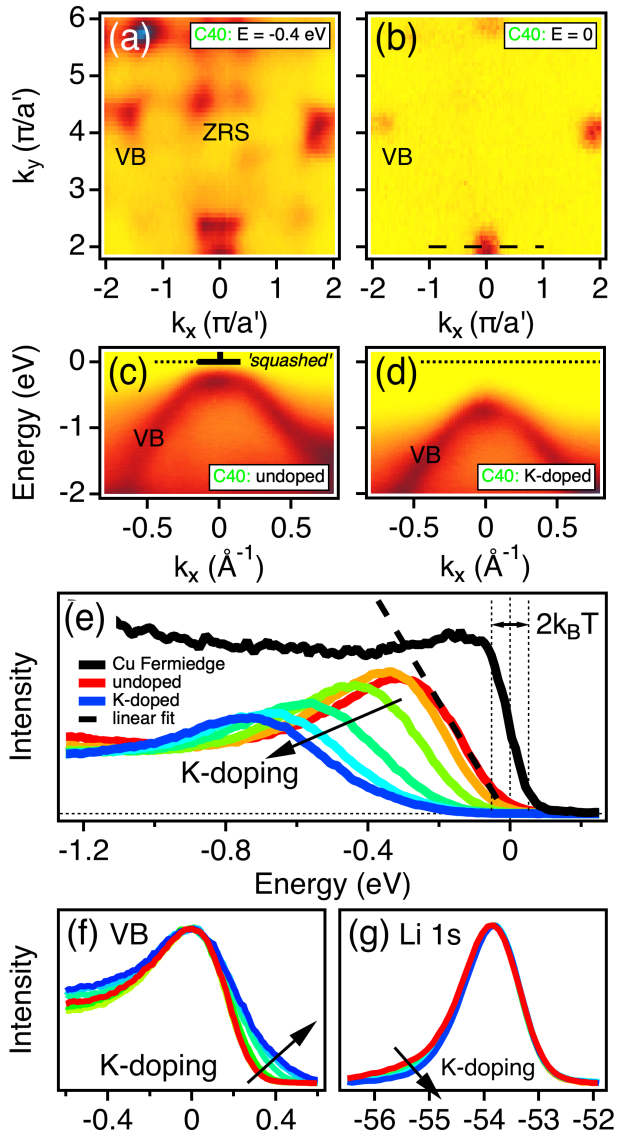

FIG. 3. ARPES CE maps of $LiCu_3O_3$ - C40 ($h\nu = 150$ eV, $T = 300$ K) at (a) $E = -0.4$ eV and (b) $E = 0 = E_F$. (c) VB dispersion along the black dotted path in (b). (d) K-deposition shifts the VB and recovers a parabolic dispersion. (e) EDC at $k_x = 0$ as a function of K-deposition. The undoped EDC (red line) exhibits a linear suppression indicative of a Coulomb gap (cf. Fermi edge of poly-crystalline Cu, black). K-doping shifts the VB towards higher energies and recovers a Lorentzian, as highlighted by the line-shape comparison in (f). (g) The (bad) metal to insulator transition of the VB is accompanied by a suppression of the shoulder in Li $1s$ [30].

(c). An energy distribution curve (EDC, red line) of the VB at $k_x = 0$ in Fig. 3 (e) appears linearly suppressed close to E_F (dashed line). While not strictly zero around $E_F \pm k_B T$ due to thermal smearing, such a linear suppression of intensity $\propto |E - E_F|$ is at odds with the Fermi liquid picture, where a Lorentzian QP lineshape $\Gamma/[(E-E_F)^2+\Gamma^2]$ with inverse QP life-time Γ, multiplied by the Fermi function, is expected. It would be, however, consistent with the bulk Efros-Shklovskii-scaling observed in transport, and thus an independent surface spectroscopic signature of the soft Coulomb gap that opens in an electron glass [19, 20, 22, 23, 33–35].

Depositing potassium (K) onto C40 induces a strong downwards band bending and electron dopes the VB, consistent with the gradual retraction of the VB from E_F observed in the EDCs of Fig. 3 (e). A line-shape comparison of all normalized and shifted EDCs in Fig. 3 (f) outlines how the initial linear onset (red) transitions to a Lorentzian line-shape (blue) upon the VB filling up and crossing the mobility edge. The filled VB is shown in panel (d) and traces a parabolic band maximum similar to what we observe for C20. Further, Fig. 3 (g) shows a consecutive suppression of the Li $1s$ high energy tail (cf. Fig. 1 f) with electron doping. This underlines the gradual depletion of the Fermi sea and a consequent reduction of core hole screening upon VB filling and the surface becoming insulating as described in Ref. 30.

Finally, we notice that despite the $\sim 40\%$ Li disorder of cleave C40 as compared to $\sim 20\%$ of C20, Figs. 1 (a) and 3 (a) show essentially equally pronounced ZRS lobes. This is consistent with ED and DFT calculations, which find the closed shell Li^+ ions to contribute no or only very little kinetic energy to the QP hopping via O $2p_{x,y}$ orbitals [18]. The system thus tends to maximize the number of unperturbed 180° Cu-O-Cu bonds each contributing one J in energy, and Li locally segregates onto one out of the two available CuO_2 sublattices (Fig. 4 a), while the ZRS stabilizes on the other. Statistical nucleation of Li and Cu atoms during crystal growth then solely demands the recurring formation of domain walls across which Li changes sub-lattice. Out of four conceivable geometries designed according to these energy criteria, ED and DFT find the alternating 3 leg ladder in Fig. 4 (b) to be energetically most compelling [18]. Taking this structure as pragmatic basis to rationalize the interplay of magnetic order and Li substitution in $LiCu_3O_3$, we calculate the electronic structure of fictitious Cu_4O_3 with all Li sites replaced by Cu(II) ions while maintaining the structure, and then introduce Li and electron correlation step-by-step. Fig. 4 (c) shows a DFT calculation of non-magnetic Cu_4O_3, yielding the metallic band structure expected for uncorrelated electrons. Introducing the Li according to the ordering geometry in Fig. 4 (b) while still refraining from correlations produces an upward shift of bands in (d), but leaves the overall band order unaltered [18]. In contrast, the experimentally determined magnetic order [18] plus Hubbard corrections open a gap in Fig. 4 (e), yet, leave this magnetic Cu_4O_3 system still metallic within a realistic 2 eV $\leq U_{\text{eff}} \leq$ 8 eV range of the effective on-site Coulomb potential. At last, only the cooperation of *both* Li *and* correlation plus magentism pushes E_F into the band gap and produces a physical picture in Fig. 4 (f) that is consistent with our ARPES experiment.

Acknowledgements.—The authors thank Helmuth Berger, Philippe Bugnon, Daniel Petitgrand, Yusuke Nomura and Silke Biermann for assistance in the initial stages of the project, as well as Sergio Ciuchi and Louk Rademaker for valuable discussions and feedback on this manuscript. S.M.

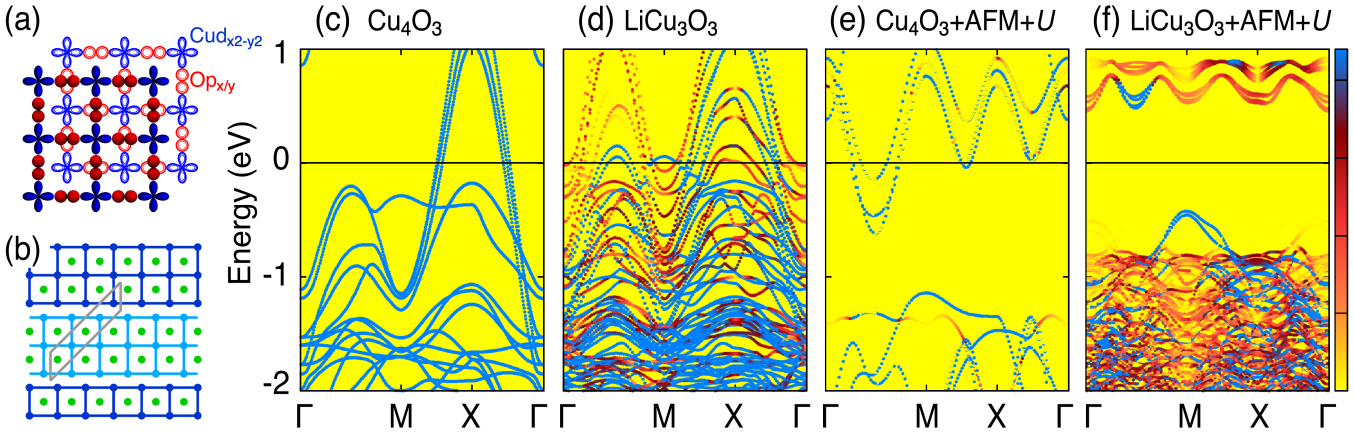

FIG. 4. (a) Decomposition of the CuO plane into two corner-sharing CuO_2 sub-lattices. The ZRS is formed from Cu $d_{x^2-y^2}$ (blue) and O $p_{x,y}$ (red) orbitals. (b) Energetically most favorable periodic ordering motif of a Cu3 plane (40% Li). Light and dark blue squares represent Cu(II)O_2 plaquettes on different sub-lattices; green dots represent Li ions. The non-magnetic UC is drawn in gray. Unfolded DFT+U band structure of (c) Cu_4O_3 without Li, magnetism and Hubbard-U; of (d) $LiCu_3O_3$, without magnetism and Hubbard-U; of (e) Cu_4O_3 with magnetism and Hubbard-U; and of (f) $LiCu_3O_3$ with AFM ordering plus Hubbard-U correlations. The color code in panels (c-f) was adapted to the one in Figs. 2 and 3, with yellow corresponding to no and blue corresponding to a strong spectral weight.

acknowledges support by the Swiss National Science Foundation under grant no. P300P2-171221. Further funding support came from the Deutsche Forschungsgemeinschaft (DFG, German Research Foundation) under Germany's Excellence Strategy through the Würzburg-Dresden Cluster of Excellence on Complexity and Topology in Quantum Matter ct.qmat (EXC 2147, Project ID 390858490) and through the Collaborative Research Centers SFB 1170 ToCoTronics (Project ID 258499086). The authors also acknowledge the Gauss Centre for Supercomputing e.V. for providing computing time on the GCS Supercomputer SuperMUC at Leibniz Supercomputing Centre. This research further used resources of the Advanced Light Source, which is a DOE Office of Science User Facility under contract no. DE-AC02-05CH11231. The research leading to these results has also received funding from the European Union's Horizon 2020 research and innovation program under the Marie Skłodowska-Curie Grant Agreement No. 897276. Additionally, this work is based on experiments performed at the Swiss spallation neutron source SINQ, Paul Scherrer Institute, Villigen, Switzerland.

* simon.moser@physik.uni-wuerzburg.de

[1] J. Ghijsen, L. H. Tjeng, J. van Elp, H. Eskes, J. Westerink, G. A. Sawatzky, and M. T. Czyzyk, Phys. Rev. B **38**, 11322 (1988).
[2] J. Zaanen, G. Sawatzky, and J. Allen, Journal of Magnetism and Magnetic Materials **54-57**, 607 (1986).
[3] F. C. Zhang and T. M. Rice, Phys. Rev. B **37**, 3759 (1988).
[4] H. Eskes and G. A. Sawatzky, Phys. Rev. Lett. **61**, 1415 (1988).
[5] H. Ebrahimnejad, G. A. Sawatzky, and M. Berciu, Nature Physics **10**, 951–955 (2014).
[6] P. W. Anderson, Phys. Rev. **79**, 350 (1950); J. B. Goodenough, Phys. Rev. **100**, 564 (1955); Journal of Physics and Chemistry of Solids **6**, 287 (1958); J. Kanamori, Journal of Physics and Chemistry of Solids **10**, 87 (1959).
[7] B. O. Wells, Z. X. Shen, A. Matsuura, D. M. King, M. A. Kastner, M. Greven, and R. J. Birgeneau, Phys. Rev. Lett. **74**, 964 (1995).
[8] Y. Mizuno, T. Tohyama, S. Maekawa, T. Osafune, N. Motoyama, H. Eisaki, and S. Uchida, Phys. Rev. B **57**, 5326 (1998).
[9] V. V. Mazurenko, S. L. Skornyakov, A. V. Kozhevnikov, F. Mila, and V. I. Anisimov, Phys. Rev. B **75**, 224408 (2007).
[10] A. A. Gippius, E. N. Morozova, A. S. Moskvin, A. V. Zalessky, A. A. Bush, M. Baenitz, H. Rosner, and S.-L. Drechsler, Physical Review B **70** (2004), 10.1103/physrevb.70.020406; S.-L. Drechsler, J. Richter, R. Kuzian, J. Málek, N. Tristan, B. Büchner, A. Moskvin, A. Gippius, A. Vasiliev, O. Volkova, A. Prokofiev, H. Rakoto, J.-M. Broto, W. Schnelle, M. Schmitt, A. Ormeci, C. Loison, and H. Rosner, Journal of Magnetism and Magnetic Materials **316**, 306 (2007), proceedings of the Joint European Magnetic Symposia.
[11] S. Moser, L. Moreschini, H.-Y. Yang, D. Innocenti, F. Fuchs, N. H. Hansen, Y. J. Chang, K. S. Kim, A. L. Walter, A. Bostwick, E. Rotenberg, F. Mila, and M. Grioni, Phys. Rev. Lett. **113**, 187001 (2014).
[12] C. P. J. Adolphs, S. Moser, G. A. Sawatzky, and M. Berciu, Phys. Rev. Lett. **116**, 087002 (2016).
[13] S. Moser, Y. Nomura, L. Moreschini, G. Gatti, H. Berger, P. Bugnon, A. Magrez, C. Jozwiak, A. Bostwick, E. Rotenberg, S. Biermann, and M. Grioni, Phys. Rev. Lett. **118**, 176404 (2017).
[14] S. Moser, Journal of Electron Spectroscopy and Related Phenomena **214**, 29 (2017).
[15] S. Hibble, J. Köhler, A. Simon, and S. Paider, Journal of Solid State Chemistry **88**, 534 (1990).
[16] R. Berger, P. Önnerud, and R. Tellgren, Journal of Alloys and Compounds **184**, 315 (1992).
[17] A. A. Bush, K. E. Kamentsev, and E. A. Tishchenko, Inorganic Materials **55**, 374 (2019).
[18] See supplemental material for details.
[19] A. L. Efros and B. I. Shklovskii, Journal of Physics C: Solid State Physics **8**, L49 (1975).

[20] A. L. Efros, Journal of Physics C: Solid State Physics **9**, 2021 (1976).

[21] J. S. Lim, J. H. Lee, A. Ikeda-Ohno, T. Ohkochi, K.-S. Kim, J. Seidel, and C.-H. Yang, Physical Review B **94**, 035123 (2016).

[22] B. I. Shklovskii and A. L. Efros, Electronic Properties of Doped Semiconductors (1984).

[23] M. Pollak, M. Ortuño, and A. Frydman, The Electron Glass (Cambridge University Press, 2012).

[24] R. Rosenbaum, Physical Review B **44**, 3599 (1991).

[25] T. Chen and B. Skinner, Physical Review B **94**, 085146 (2016).

[26] D. Joung and S. I. Khondaker, Physical Review B **86**, 235423 (2012), arXiv:1210.1876.

[27] N. Papadopoulos, G. A. Steele, and H. S. J. van der Zant, Phys. Rev. B **96**, 235436 (2017).

[28] V. Y. Butko, J. F. DiTusa, and P. W. Adams, Physical Review Letters **84**, 1543 (2000).

[29] B. Rachmilowitz, H. Zhao, Z. Ren, H. Li, K. H. Thomas, J. Marangola, S. Gao, J. Schneeloch, R. Zhong, G. Gu, C. Flindt, and I. Zeljkovic, npj Quantum Materials **5**, 72 (2020).

[30] S. Doniach and M. Sunjic, Journal of Physics C: Solid State Physics **3**, 285 (1970).

[31] P. D. C. King, T. D. Veal, and C. F. McConville, Physical Review B **77**, 125305 (2008).

[32] Apart from an *Umklapp* band (UB) that is observed only in $LiCu_2O_2$ [13].

[33] M. Pollak, Discussions of the Faraday Society **50**, 13 (1970).

[34] S. Souma, L. Chen, R. Oszwałdowski, T. Sato, F. Matsukura, T. Dietl, H. Ohno, and T. Takahashi, Scientific Reports **6**, 1 (2016).

[35] Y.-H. Song, Z.-Y. Jia, D. Zhang, X.-Y. Zhu, Z.-Q. Shi, H. Wang, L. Zhu, Q.-Q. Yuan, H. Zhang, D.-Y. Xing, and S.-C. Li, Nature Communications **9**, 4071 (2018), arXiv:1711.07286.